The Price of Synchrony: Evaluating the Resistive Losses in Synchronizing Power Networks

Emma Tegling, Bassam Bamieh, *Fellow, IEEE*, and Dennice F. Gayme, *Senior Member, IEEE*

***Abstract*—This paper investigates the resistive power losses that are incurred in keeping a network of synchronous generators in a synchronous state. These losses arise due to the transient power-flow fluctuations that occur when the system is perturbed from a synchronous state by a small transient event or in the face of persistent stochastic disturbances. We call these losses the "price of synchrony," as they reflect the real power-flow costs incurred in resynchronizing the system. In the case of small fluctuations at each generator node, we show how the total network's resistive losses can be quantified using an $\mathcal{H}_2$ norm of a linear system of coupled swing equations subject to distributed disturbances. This norm is shown to be a function of transmission-line and generator properties, to scale unboundedly with network size, and to be weakly dependent on the network topology. This conclusion differentiates the price of synchrony from typical power systems stability notions, which show highly connected networks to be more coherent and, thus, easier to synchronize. In particular, the price of synchrony is more dependent on a network's size than its topology. We discuss possible implications of these results in terms of the design of future power grids, which are expected to have highly distributed generation resources leading to larger networks with the potential for greater transient losses.**

***Index Terms*—Distributed control, large-scale networks, oscillator networks, power networks, power system dynamics system performance.**

I. Introduction

THE electric power system is undergoing rapid changes. The power grid of the future is expected to have higher levels of uncertainty from renewable energy sources [1], changing load patterns [2], and increasingly distributed electricity generation [3]. Many of these changes can affect the stability of the power network. The inherent variability of solar and wind energy, for example, is likely to produce more frequent and higher amplitude disturbances. Such disturbances, along with greater distribution of both conventional and renewable generation resources, have the potential to affect rotor-angle stability, which is the ability of the power grid to recover synchrony after a disturbance [4]. Synchrony, in this context, refers to the alignment of the frequency and phase of all generators within a particular power network. In other words, it is when all of the frequencies are equal [5] and the phase differences are at an equilibrium state corresponding to balanced power flows throughout the network. Maintaining synchrony in a network thus depends on its ability to sustain or restore this condition when it is subjected to disturbances from this nominal operating point.

Synchronous stability properties of power systems are typically studied using a so-called network reduced model where power loads are modeled as equivalent impedances that are absorbed into the "transmission lines" of the reduced network, see, for example, [5]–[9] and the references therein. The resulting system is a set of coupled swing equations that describe the dynamics of a network of generators connected by these lines. This system is then analyzed to determine conditions under which the synchronized state is stable, see, for example, [5] and [10]. These analyses are related to the well-studied transient stability problem, see, for example, [11], which refers to the ability of a system to return to a stable operating condition after a large angle disturbance.

A recent research trend has been to analyze synchronous stability properties of power systems using tools from systems and control theory. The associated literature is vast and here we highlight only a subset of this research. For example, a series of works draws connections between power grids and coupled Kuramoto oscillators [10], [12]–[14]. The nonuniform Kuramoto oscillator modeling framework provides a first-order approximation of the network reduced model. Dörfler and Bullo [13], [14] exploit the properties of this well-studied system to provide network parameter-dependent analytical conditions for frequency and phase synchronization in power networks. In a related work [15], these authors also make connections between network reduced models and the structure preserving network model of Bergen and Hill [16]. Similar first-order models have been used to investigate the effects of power-flow scheduling and increasing power network interconnectivity (i.e., adding transmission lines) on the rate of convergence [17].

The control design for synchronizing networks of LC-oscillators has also been investigated in [18] and [19], where synchronization is defined in terms of voltage differences between connected nodes rather than phase differences. These authors employ an $\mathcal{H}_2$ system norm as a performance metric for control design. As will be described later, the current work also uses an $\mathcal{H}_2$ norm-based performance metric. However, the system dynamics and the output are defined differently and, therefore, these are two distinct performance metrics.

Manuscript received March 9, 2014; revised October 17, 2014; accepted November 14, 2014. Date of publication April 14, 2015; date of current version September 14, 2015. This work was supported in part by AFOSR under Grant FA9550-10-1-0143 and in part by the National Science Foundation under Grant ECCS 1230788 and INSPIRE Award PHY-1344069.

E. Tegling is with the Department of Mechanical Engineering, Johns Hopkins University, Baltimore, MD 21218 USA, and also with the School of Electrical Engineering, KTH Royal Institute of Technology, Stockholm SE-100 44, Sweden (e-mail: tegling@kth.se).

B. Bamieh is with the Department of Mechanical Engineering, University of California at Santa Barbara, Santa Barbara, CA 93106 USA (e-mail: bamieh@engineering.ucsb.edu).

D. F. Gayme is with the Department of Mechanical Engineering, Johns Hopkins University, Baltimore, MD 21218 USA (e-mail: dennice@jhu.edu).

Digital Object Identifier 10.1109/TCNS.2015.2399193

In this paper, we formulate a new problem and study synchrony in power networks in the context of network performance rather than stability. For this purpose, we assume that the network is synchronously stable, that is, the system is at a stable operating condition and will return to this synchronized state after being subjected to small disturbances. We then focus on the *control effort* required to maintain or return to synchrony. We define this control effort as follows. Lack of synchrony leads to nonequilibrium circulating currents [20] passing between generators whose angles no longer correspond to the values associated with their nominal phase differences. These nonequilibrium current fluctuations act as a signaling mechanism that indicates that the system needs to be resynchronized and results in transient resistive losses over the power lines. These losses are essentially the cost of using power-flow fluctuations (as opposed to, for example, a communications infrastructure) as the signaling mechanism to achieve synchronization between generators. It is in this sense that we refer to these losses as a control effort and as the "price of synchrony." We point out that other signaling mechanisms [21] based on information transmission can be used for synchronization, and these would not incur the transient power losses we investigate. However, in this paper, we do not consider such systems, and focus instead on how the current scheme of using fluctuating power flows as the synchronization signal could scale to larger networks.

This work investigates the transient power losses described above using a reduced network system of synchronous generators subject to disturbances. We show that the total transient power losses due to nonzero line resistances can be quantified through the $\mathcal{H}_2$ norm of an input–output system of coupled swing equations with an appropriately defined output. This $\mathcal{H}_2$ norm can be interpreted as the average (per time) transient power losses that arise due to either small persistent stochastic disturbances, or as the total (over all time) transient power losses due to a small transient event. We determine expressions for this norm using so-called grounded Laplacians [22], [23] where the neutrally stable network-mean mode is removed. This mode is unobservable based on the system output associated with the performance objective defined herein. Physically, this reduction corresponds to grounding one of the generator nodes and modeling this node as an infinite bus with fixed states.

Our main result proves that the total transient resistive power losses in a network of identical generators depend on a generalized ratio between weighted graph Laplacians defined based on the line resistances and reactances for the reduced network. We provide bounds on this generalized ratio, which show that the transient losses grow unboundedly with the number of network nodes. In the special case of a network with all edges having identical resistance to reactance ratios, the losses scale directly with the number of nodes and are entirely independent of the network topology. In other words, for this special case, highly connected and loosely connected networks with the same number of nodes incur the same resistive power losses in recovering synchrony. In more general network settings, the losses are affected by network topology, but this dependence remains weak and the price of synchrony depends more on the size of the network than its connectivity. Therefore, even though the transient power losses that arise during synchronization are typically a small percentage of the total real power flow, our results (based on a simplified network model) indicate that these losses may become significant as power networks evolve toward increasingly distributed systems. Furthermore, merely adding links to the network to increase connectivity is unlikely to alleviate the increases in transient power losses as the network grows.

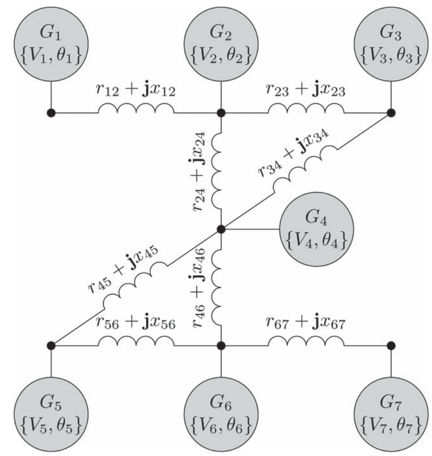

Fig. 1. Example of a network of $N = 7$ generator nodes.

In order to put the results for the previously described special cases in a larger context, we also provide some generalizations of the theory for systems of heterogeneous generators. In particular, we examine the problem of adding a generator to an existing network. These results indicate that the marginal losses incurred by adding a well-damped, low-inertia generator to the system are small compared to those arising through the addition of a poorly damped, high-inertia one. This generator parameter dependence is particularly relevant in the face of increasingly distributed generation in low-voltage (LV) grids, which typically have higher line resistances (i.e., greater real power losses). Numerical examples also demonstrate that careful selection and placement of different generators can be used to reduce or increase transient losses. These effects are, however, weaker than the effect of network size and, in practice, strategic configuration of generators is unlikely to mitigate increases in the transient losses due to larger networks.

The remainder of this paper is organized as follows. Section II introduces the problem formulation and describes connections between the current work and distributed control theory. Section III derives algebraic expressions for the resistive losses and provides the main results. A discussion of generalizations and bounds on the $\mathcal{H}_2$ norm is provided in Section IV. Section V contains some numerical examples to illustrate the theory. Finally, we summarize the main findings and discuss directions for future work in Section VI.

II. Problem Formulation

Consider a network of N nodes (buses) and a set of edges (network lines) $\mathcal{E}$, as depicted in Fig. 1 for a system where $N = 7$. Throughout this section, we assume a Kron-reduced network model (see, for example, [9], [11], and [24]) where loads are modeled as impedances that are absorbed into the network lines. Thus, at every node $i = 1, \ldots, N$, there is a generator with inertia constant M_i, damping coefficient β_i, voltage magnitude $|V_i|$, and voltage phase angle θ_i. In the absence of external control, the dynamics of the i^{th} generator can be described using the following classical machine model [6]:

$$M_i\ddot{\theta}_i + \beta_i\dot{\theta}_i = P_{m,i} - P_{e,i} \qquad \forall\, i = 1, 2, \ldots, N \tag{1}$$

where $P_{m,i}$ is the mechanical power input from the turbine. $P_{e,i}$ is the electrical power flow out of the i^{th} generator (i.e., the real power injected into the grid), which is given by

$$P_{e,i} = \bar{g}_i|V_i|^2 + \sum_{j\sim i} g_{ij}|V_i|\,|V_j|\cos(\theta_i - \theta_j) + \sum_{j\sim i} b_{ij}|V_i|\,|V_j|\sin(\theta_i - \theta_j). \tag{2}$$

Here, $j \sim i$ indicates the existence of a line (edge $\mathcal{E}_{ij}$) connecting nodes i and j in the Kron-reduced network model. g_{ij} and b_{ij} are, respectively, the conductance and susceptance associated with edge $\mathcal{E}_{ij}$ and $\bar{g}_i$ is the shunt conductance of node i.

In order to simplify the notation, we define the bus admittance matrix $Y \in \mathbb{C}^{n\times n}$ of the reduced network as

$$Y_{ij} := \begin{cases} \bar{g}_i + \sum\limits_{k\sim i}(g_{ik} - \mathbf{j}b_{ik}), & \text{if } i = j \\ -(g_{ij} - \mathbf{j}b_{ij}), & \text{if } i \neq j \text{ and } j \sim i \\ 0 & \text{otherwise.} \end{cases}$$

Y can be partitioned into a real and an imaginary part such that

$$Y = (L_G + \bar{g}) - \mathbf{j}L_B \tag{3}$$

where L_G denotes the conductance matrix, L_B denotes the susceptance matrix, and $\bar{g} := \operatorname{diag}\{\bar{g}_i\}$ is the associated diagonal matrix of shunt conductances. The matrices L_B and L_G are Laplacians of the weighted network graphs respectively defined by the susceptances b_{ij} and conductances g_{ij} of the lines in the Kron-reduced network.

We now further approximate the power system model (1) and (2) by linearizing the system around a stable operating point $[\theta^*, \omega^*]^T$, which WLOG we can transfer to the origin through a change of variables. This linearization allows us to investigate the effects of small disturbances or persistent small amplitude noise within a small neighborhood of the operating point. It is therefore well suited to analyze the effects of small phase angle and frequency changes associated with the system returning to a synchronous state (stable operating point) after a small transient event or in the face of small persistent disturbances.

The standard linear power-flow assumptions include constant voltages $|V_i| = 1$ for every bus i, and retaining only the linear terms in (2), which leads to

$$P_{e,i} \approx \sum_{j\in\mathcal{N}} b_{ij}[\theta_i - \theta_j]. \tag{4}$$

See, for example, [25] for a detailed analysis of the applicability of such assumptions. Substituting (4) into (1) leads to

$$M_i\ddot{\theta}_i + \beta_i\dot{\theta}_i \approx -\sum_{j\in\mathcal{N}} b_{ij}[\theta_i - \theta_j] + P_{m,i} \tag{5}$$

which we can rewrite in state space form as follows:

$$\frac{\mathrm{d}}{\mathrm{d}t}\begin{bmatrix}\theta\\ \omega\end{bmatrix} = \begin{bmatrix} 0 & I \\ -\mathcal{M}^{-1}L_B & -\mathcal{M}^{-1}\mathcal{B}\end{bmatrix}\begin{bmatrix}\theta\\ \omega\end{bmatrix} + \begin{bmatrix}0\\ \mathcal{M}^{-1}\end{bmatrix}\mathrm{w} \tag{6}$$

where $\mathcal{M} = \operatorname{diag}\{M_i\}$, $\mathcal{B} = \operatorname{diag}\{\beta_i\}$, and we have assumed that $P_{m,i}$ is a constant that can be lumped into the input w.

A. *System Performance*

As mentioned in the introduction, our concern is not to characterize the stability of the system (6) but rather to evaluate the transient power flows that occur as the system resynchronizes after a small disturbance from a nominal operating condition or in the face of persistent small-amplitude disturbances. We therefore assume that the system matrices are such that the dynamics are stable around the equilibrium manifold for which all phases are equal. We now define the system output (measurement) needed to evaluate the real power losses arising from the fluctuating phase-angle differences associated with small excursions from the stable operating point.

The real power loss over an edge $\mathcal{E}_{ij}$ is $P_{ij} = g_{ij}|V_i - V_j|^2$. If we enforce the linear power-flow assumptions and retain only the terms that are quadratic in the state variables, then standard trigonometric identities can be used to obtain the approximation $P_{ij} \approx g_{ij}(\theta_i - \theta_j)^2$ for this flow. Since we are regarding θ_i as the deviation from the i^{th} generator's nominal operating point, this power flow is equivalent to the resistive power loss over the edge as the system resynchronizes. The corresponding sum of instantaneous, transient resistive power losses over all links in the network can then be approximated as

$$\mathbf{P}_{\text{loss}} = \sum_{i\sim j} g_{ij}(\theta_i - \theta_j)^2. \tag{7}$$

We can now make use of the conductance matrix L_G to rewrite (7) as the quadratic form $\mathbf{P}_{\text{loss}} = \theta^* L_G \theta$. Since L_G is a weighted graph Laplacian, which is positive semidefinite, we can define a system output

$$y = [\,C_1 \quad 0\,]\begin{bmatrix}\theta\\ \omega\end{bmatrix} \tag{8}$$

where $C_1 := L_G^{1/2}$ is the unique positive semidefinite square root of L_G. It is then easy to see that $\mathbf{P}_{\text{loss}} = y^* y$.

For ease of reference, we rewrite the state dynamics (6) and the output equation (8) together as the MIMO LTI system

$$\frac{\mathrm{d}}{\mathrm{d}t}\begin{bmatrix}\theta\\ \omega\end{bmatrix} = \begin{bmatrix} 0 & I \\ -\mathcal{M}^{-1}L_B & -\mathcal{M}^{-1}\mathcal{B}\end{bmatrix}\begin{bmatrix}\theta\\ \omega\end{bmatrix} + \begin{bmatrix}0\\ \mathcal{M}^{-1}\end{bmatrix}\mathrm{w} \tag{9a}$$

$$y = \begin{bmatrix} L_G^{\frac{1}{2}} & 0\end{bmatrix}\begin{bmatrix}\theta\\ \omega\end{bmatrix}. \tag{9b}$$

This LTI system is a *Linear Quadratic* approximation of the full nonlinear problem in the sense that the dynamics have been linearized around an equilibrium corresponding to the condition where the system power flow is balanced and all generators are operating at a nominal frequency. The instantaneous resistive power losses are quadratically approximated by the (square of the) Euclidean norm of the output signal y. We next describe several interpretations of the $\mathcal{H}_2$ norm of the system (9) in terms of the total transient resistive losses (price of synchrony).

Remark 1: The system (9a) represents a linearization of the swing dynamics (6) which assumes that line resistances are negligible, while the output (9b) measures the effect of nonzero resistances given the system trajectories arising from the dynamics of (9a).

B. $\mathcal{H}_2$ Norm Interpretations for Swing Dynamics

The LTI system (9) is formulated so that the square of the Euclidean norm of the output $y(t)^*y(t)$ is the instantaneous resistive power loss at time t. The $\mathcal{H}_2$ norm of this system can be interpreted as the average (per time t) power loss in a setting with persistent disturbances, or alternatively as the total (over all time) power loss due to a transient event. These interpretations of the $\mathcal{H}_2$ norm are standard, but we recap them here in the context of the particular physical scenarios for the power network setting considered in this paper.

Denote by H the LTI system (9), and consider the following three scenarios.

1) *Response to a white stochastic input*. When the input w is a white second-order process with unit covariance (i.e., $\mathrm{E}\{\mathrm{w}(\tau)\mathrm{w}^*(t)\} = \delta(t-\tau)I$), the (squared) $\mathcal{H}_2$ norm of the system is the steady-state total variance of all output components, that is

$$\|H\|_{\mathcal{H}_2}^2 = \lim_{t\to\infty} \mathrm{E}\left\{y^*(t)y(t)\right\}.$$

For the swing dynamics (9), the disturbance vector can be thought of as persistent stochastic forcing at each generator. These disturbances, which are uncorrelated across generators, can be due to uncertainties in local generator conditions, such as changes in local load or supplied mechanical power. The variance of the output is exactly the expectation of the total (over the entire network) instantaneous power loss due to line resistances.

2) *Response to a random initial condition*. With zero input and an initial condition that is a random variable x_o with correlation $\mathrm{E}\{x_o x_o^*\} = BB^*$, the $\mathcal{H}_2$ norm is the time integral

$$\|H\|_{\mathcal{H}_2}^2 = \int_0^\infty \mathrm{E}\left\{y^*(t)y(t)\right\}\,\mathrm{d}t$$

of the resulting response y.

The interpretation for (9) is as follows. Since $BB^* = \begin{bmatrix} 0 & 0 \\ 0 & \mathcal{M}^{-2} \end{bmatrix}$, which is diagonal, the initial condition corresponds to each generator having a random initial velocity perturbation that is uncorrelated across generators and zero initial phase perturbation. In this case, $\|H\|_{\mathcal{H}_2}^2$ quantifies the total (over all time and the entire network) expected resistive power losses due to the system returning to a synchronized state.

3) *Sum of responses to impulses at all inputs*. Let e_i refer to the vector with a 1 in the i^{th} component and zero everywhere else. Consider N experiments where in each, the system is fed an impulse at the i^{th} input channel, that is, $\mathrm{w}_i(t) = e_i\delta(t)$. Denote the corresponding output by y_i. The (squared) $\mathcal{H}_2$ norm is then the sum of the L_2 norms of these outputs, that is

$$\|H\|_{\mathcal{H}_2}^2 = \sum_{i=1}^N \int_0^\infty y_i^*(t)y_i(t)\,\mathrm{d}t.$$

A stochastic version of this scenario corresponds to a system where the inputs w_i can occur with equal probability. Under this assumption, $\|H\|_{\mathcal{H}_2}^2$ becomes the expected total power loss given these inputs.

The corresponding interpretation for (9) is when each generator is subject to impulse force disturbances (since w enters the momentum equation of each generator), then $\|H\|_{\mathcal{H}_2}^2$ is the total power loss that is incurred during resynchronization.

C. Relations to Network Coherence

The LTI model (9a) is very similar to the model of vehicular dynamics studied in [26]. The notion of *network coherence* studied there can be translated in the present context of power networks as quantifying how tightly the phases of all generators drift together. More precisely the following quantity:

$$\mathrm{E}\left\{\left(\theta_i - \frac{1}{N}\sum\nolimits_{j=1}^N \theta_j\right)^2\right\} \tag{10}$$

expresses the variance of the deviation of the i^{th} node from the average over all nodes in the network. This quantity is never zero when there are stochastic disturbance inputs, even in a stable power network. Larger relative phase deviation variances reflect a more disordered network while smaller variances imply a more coherent network.

The asymptotic behavior of the disorder measure (10) as the network size N increases was studied in [26] for regular network structures such as multidimensional tori and their variations. The basic trend is the intuitive one that more connected networks tend to be more coherent and vice-versa. In that analysis, however, the control cost was considered as *per vehicle*, while in the present context, it is the total or aggregate transient resistive power loss over the entire network that is of concern. Thus, although the two settings have analogous dynamics, the performance objectives differ. We point out that the disorder measure (10) is not the Euclidean norm of the output y defined in (9b). In other words, the amount of phase disorder in a network as measured by (10) is not necessarily related to resistive power losses and, in particular, may not scale similarly with network size N. While networks with high phase coherence may be desirable for other reasons (such as stability of the nonlinear model), the results to be presented shortly indicate that the price of synchrony (total transient resistive power losses) can be large even in highly coherent networks.

III. Evaluating Resistive Losses

In this section, we derive a formula for the $\mathcal{H}_2$ norm of the system (9) in terms of the system matrices and parameters. We then consider the implications for some important special cases.

Throughout this section, we assume identical generators, that is, $\mathcal{M} = MI$ and $\mathcal{B} = \beta I$.

A. System Reduction

As previously discussed, L_G and L_B are graph Laplacians. They therefore share the eigenvector $v = \mathbf{1}$, with all components equal to 1, and the associated zero eigenvalue, that is

$$L_B\mathbf{1} = L_G\mathbf{1} = 0.$$

The zero eigenvalue implies that these matrices are singular and that the system (9) is not asymptotically stable. However, as shown in the Appendix, this mode is not observable from the performance output y. If the network is connected, the remaining eigenvalues are stable and therefore the system has a finite $\mathcal{H}_2$ norm. In order to properly define the $\mathcal{H}_2$ norm of (9), we perform a system reduction procedure that effectively removes the unobservable mode at 0 and enables us to investigate a reduced system that is asymptotically stable.

Following the approach in [23], we derive the reduced system by first defining a reference state $k \in \{1, \ldots, N\}$. We denote the reduced or *grounded* Laplacians that arise from deleting the k^{th} rows and columns of L_G and L_B, respectively, as $\tilde{L}_G$ and $\tilde{L}_B$. The states of the reduced system $\tilde{\theta}$ and $\tilde{\omega}$ are then obtained by discarding the k^{th} elements of each state vector. This leads to a system that is equivalent to one in which $\theta_k = \omega_k \equiv 0$ for some node $k \in \{1, 2, \ldots, N\}$. The physical interpretation of the reduced system is that the k^{th} node is connected to ground. We call the resulting reduced, or grounded, system $\tilde{H}$ and rewrite it as

$$\begin{aligned}\frac{\mathrm{d}}{\mathrm{d}t}\begin{bmatrix}\tilde{\theta}\\ \tilde{\omega}\end{bmatrix} &= \begin{bmatrix}0 & I\\ -\frac{1}{M}\tilde{L}_B & -\frac{\beta}{M}I\end{bmatrix}\begin{bmatrix}\tilde{\theta}\\ \tilde{\omega}\end{bmatrix} + \begin{bmatrix}0\\ \frac{1}{M}I\end{bmatrix}\tilde{\mathrm{w}} \qquad (11a)\\ &=: A\tilde{\phi} + B\tilde{\mathrm{w}};\\ \tilde{y} &= \begin{bmatrix}\tilde{L}_G^{\frac{1}{2}} & 0\end{bmatrix}\begin{bmatrix}\tilde{\theta}\\ \tilde{\omega}\end{bmatrix} =: C\tilde{\phi} \qquad (11b)\end{aligned}$$

where $\tilde{\phi} = [\tilde{\theta} \quad \tilde{\omega}]^T$. Assuming a network where the underlying graph is connected, the grounded Laplacians $\tilde{L}_G$ and $\tilde{L}_B$ are positive definite Hermitian matrices (see, for example, [22]). All of the eigenvalues of system $\tilde{H}$ are thus strictly in the left half of the complex plane and the input–output transfer function from $\tilde{\mathrm{w}}$ to $\tilde{y}$ has a finite $\mathcal{H}_2$ norm.

B. $\mathcal{H}_2$ Norm Calculation

The squared $\mathcal{H}_2$ norm of the system $\tilde{H}$ is given by

$$\|\tilde{H}\|^2_{\mathcal{H}_2} = \mathrm{tr}(B^*\tilde{X}B)$$

where $\tilde{X}$ is the observability Gramian that can be obtained from the Lyapunov equation $A^*\tilde{X} + \tilde{X}A = -C^*C$. Expanding this equation for the system $\tilde{H}$ in (11) leads to

$$\begin{bmatrix}0 & -\frac{1}{M}\tilde{L}_B\\ I & -\frac{\beta}{M}I\end{bmatrix}\begin{bmatrix}\tilde{X}_1 & \tilde{X}_0\\ \tilde{X}_0^* & \tilde{X}_2\end{bmatrix} + \begin{bmatrix}\tilde{X}_1 & \tilde{X}_0\\ \tilde{X}_0^* & \tilde{X}_2\end{bmatrix}\begin{bmatrix}0 & I\\ -\frac{1}{M}\tilde{L}_B & -\frac{\beta}{M}I\end{bmatrix} = -\begin{bmatrix}\tilde{L}_G & 0\\ 0 & 0\end{bmatrix}$$

from which we extract the following two equations:

$$X_0 - \frac{\beta}{M}\tilde{X}_2 + \tilde{X}_0^* - \tilde{X}_2\frac{\beta}{M} = 0 \qquad (12a)$$

$$-\frac{1}{M}\tilde{L}_B\tilde{X}_0^* - \tilde{X}_0\frac{1}{M}\tilde{L}_B = -\tilde{L}_G. \qquad (12b)$$

Then, using (12a), it is straightforward to compute $\frac{\beta}{M}\mathrm{tr}(\tilde{X}_2) = \mathrm{tr}(\mathrm{Re}\{\tilde{X}_0\})$. Equation (12b) can be rearranged to yield

$$\tilde{L}_B\tilde{X}_0^*\tilde{L}_B^{-1} + \tilde{X}_0 = M\tilde{L}_G\tilde{L}_B^{-1}$$

where we make use of the fact that $\tilde{L}_B$ is nonsingular. Combining these expressions and using standard matrix trace relationships leads to the following expression:

$$\mathrm{tr}(\tilde{X}_2) = \frac{M^2}{2\beta}\mathrm{tr}\left(\tilde{L}_B^{-1}\tilde{L}_G\right). \qquad (13)$$

Finally, noting that $\mathrm{tr}(B^*\tilde{X}B) = (1/M^2)\mathrm{tr}(\tilde{X}_2)$, we derive the following Lemma.

Lemma 3.1: The squared $\mathcal{H}_2$ norm of the input–output mapping of the system (11) is given by

$$\|\tilde{H}\|^2_{\mathcal{H}_2} = \frac{1}{2\beta}\mathrm{tr}\left(\tilde{L}_B^{-1}\tilde{L}_G\right) \qquad (14)$$

where $\tilde{L}_B$ and $\tilde{L}_G$ are the grounded Laplacians obtained using the previously described procedure and β is each generator's self damping.

The choice of grounded node k has no influence on the $\mathcal{H}_2$ norm given in (14). We illustrate this point through the following lemmas, which are used to derive the main result stated in Theorem 3.4.

Lemma 3.2: Let H denote the input–output mapping (9) with $\mathcal{M} = MI$ and $\mathcal{B} = \beta I$ and $\tilde{H}$ denote the corresponding reduced system (11). Then, the norm $\|H\|^2_{\mathcal{H}_2}$ exists and

$$\|H\|^2_{\mathcal{H}_2} = \|\tilde{H}\|^2_{\mathcal{H}_2}.$$

Proof: See the Appendix. ■

Lemma 3.3: Let $\tilde{L}_G$ and $\tilde{L}_B$ be the reduced, or grounded, Laplacians obtained by deleting the k^{th} row and column of L_G and L_B respectively. Then

$$\mathrm{tr}\left(\tilde{L}_B^{-1}\tilde{L}_G\right) = \mathrm{tr}\left(L_B^{\dagger}L_G\right) \qquad (15)$$

where † denotes the Moore–Penrose pseudoinverse.

Proof: See the Appendix. ■

The result can now be stated in the following theorem, which was also independently derived in [27].

Theorem 3.4: Given a system of N generators with equal damping and inertia coefficients $\beta_i = \beta$ and $M_i = M$, $\forall i \in \{1, \ldots, N\}$ whose input–output response is given by (9). The squared $\mathcal{H}_2$ norm of the system is given by

$$\boxed{\|H\|^2_{\mathcal{H}_2} = \frac{1}{2\beta}\mathrm{tr}\left(L_B^{\dagger}L_G\right).} \qquad (16)$$

Thus, the total transient losses of the system are a function of what we call the generalized Laplacian ratio of L_G to L_B.

Proof: The result follows directly from Lemmas 3.1–3.3. ■

In (9), we assumed that the mechanical input $P_{m,i}$ to each generator i is lumped into the input w. If instead, one chooses to scale the input by the generator's inertia, that is, define $\mathrm{w}' := (1/M)\mathrm{w}$ and $B' := [0 \quad I]^T$, then the squared $\mathcal{H}_2$ norm of the resulting system can be constructed in an analogous manner, as shown in the following Corollary.

Corollary 3.5: Consider the modified input–output mapping

$$\frac{d}{dt}\begin{bmatrix}\theta \\ \omega\end{bmatrix} = \begin{bmatrix} 0 & I \\ -\frac{1}{M}L_B & -\frac{\beta}{M}I\end{bmatrix}\begin{bmatrix}\theta \\ \omega\end{bmatrix} + \begin{bmatrix}0 \\ I\end{bmatrix}\mathrm{w}' \tag{17}$$

$$y = \begin{bmatrix} L_G^{\frac{1}{2}} & 0\end{bmatrix}\begin{bmatrix}\theta \\ \omega\end{bmatrix}.$$

The $\mathcal{H}_2$ norm (squared) of this system is

$$\|H'\|^2_{\mathcal{H}_2} = \frac{M^2}{2\beta}\mathrm{tr}\left(L_B^{\dagger}L_G\right).$$

Proof: Following the proof of Lemma 3.1, we first note that for this modified system $\mathrm{tr}(B'^*\tilde{X}B') = \mathrm{tr}(\tilde{X}_2)$. The result then follows directly from Lemmas 3.2 and 3.3. ■

Theorem 3.4 states that the price of synchrony (transient resistive losses) is proportional to what can be thought of as a generalized ratio between the conductance and susceptance matrices. The ratio of line conductances to susceptances or, equivalently, resistances to reactances is generally small for transmission systems and is therefore often neglected in power flow calculations [25] and stability analyses. However, the matrix trace operation in (16) implies that the transient resistive losses increase with network size (number of generators). Therefore, transient resistive losses may become significant in large networks with highly distributed generation even when line resistances are small. In LV distributed generation networks where the resistance to reactance ratios are higher than in transmission systems,[1] this trend would be doubly problematic, as both the network size and this ratio are larger. The next section explores the effect of network size directly for the important special case of equal line ratios.

C. Special Case: Equal Line Ratios

We now consider the special case when the generalized Laplacian ratio in (16) is a scalar matrix αI, where

$$\alpha := \frac{g_{ij}}{b_{ij}} = \frac{r_{ij}}{x_{ij}}.$$

In other words, all lines in the system $\mathcal{E}_{ij} \in \mathcal{E} \;\forall\; i \sim j$ have equal resistance to reactance ratios. This assumption implies $L_G = \alpha L_B$. Thus, by Lemmas 3.1 and 3.2

$$\|H\|^2_{\mathcal{H}_2} = \frac{1}{2\beta}\mathrm{tr}\left(\tilde{L}_B^{-1}\alpha\tilde{L}_B\right) = \frac{\alpha}{2\beta}(N-1) \tag{18}$$

which is the result presented in [29]. This result is remarkable in that it says that for this special case, the size of the transient losses depends only on the network's size and is entirely independent of its topology.

Remark 2: If we instead define a weighted mean $\overline{\alpha}$ of the line ratios $\alpha_{ij} = (g_{ij}/b_{ij})$ for all $\mathcal{E}_{ij}$ in the system, the result in (18) can be generalized to a system with heterogeneous line ratios [27].

Remark 3: A choice of $\alpha_{\max} \geq (g_{ij}/b_{ij})$ for all edges $\mathcal{E}_{ij} \in \mathcal{E}$ can be used to define a conservative bound from (18) [27]. One can similarly define a lower bound $\alpha_{\min} \leq (g_{ij}/b_{ij})$ to bound the $\mathcal{H}_2$ norm of the system as

$$\frac{\alpha_{\min}}{2\beta}(N-1) \leq \|H\|^2_{\mathcal{H}_2} \leq \frac{\alpha_{\max}}{2\beta}(N-1) \tag{19}$$

where $\alpha_{\min(\max)}$ are the smallest (largest) of the line ratios [27]. These bounds also increase unboundedly with the number of generators and are independent of the network topology.

It is worth noting that the topology independence in (18) and the bounds discussed in Remark 3 are in contrast to measures of power system stability and performance metrics, such as network coherence and damping. For example, the topology of the system plays an important role in determining whether a system of this kind can synchronize [12], [13], [26], [30]. The network connectivity of a power system is also directly related to its rate of convergence and damping properties [17]. One intuitive explanation for the price of synchrony being independent of network topology for the equal line ratio case is as follows. We expect a highly connected network to have much more phase coherence than a loosely connected network with the same number of nodes. Consequently, the power flows per link in a highly connected network are relatively small, but there are many more links than in the loosely connected network. Thus, in the aggregate, the total transient power losses are the same for both networks. A more coherent network is, however, more stable.

The equal line ratio assumption is not unreasonable for power systems, as the ratio of resistances to reactances of typical transmission links tend to lie within a small interval. A recent study [5] found that the node degrees of Kron-reduced networks tend to be much more uniform than those of the full power networks that they are derived from. Those results suggest that the "lines" of such reduced systems are also more uniform than those found in actual power networks and, therefore, the equal line ratio assumption is suitable for the reduced network considered here.

IV. Generalizations and Bounds

In this section, we provide bounds on the expression (16) and discuss their implications. We also address the more general case of systems with nonidentical generators.

A. Loss Bounds

As previously mentioned, the term $\mathrm{tr}(L_B^{\dagger}L_G)$ in Theorem 3.4 can be interpreted as a generalized ratio between the network's conductance matrix L_G and its susceptance matrix L_B, that is, the real and imaginary part of the bus admittance matrix without the shunt conductances $(Y - \overline{g})$. We denote the respective

[1] Typically, this ratio is 1/16 in 400 kV lines but 2/3 in 11 kV systems [28].

eigenvalues of L_G as $\lambda_N^G \geq \ldots \geq \lambda_2^G > 0$ and of L_B as $\lambda_N^B \geq \ldots \geq \lambda_2^B > 0$. The generalized ratio of these two Laplacians can then be lower bounded in terms of these eigenvalues as

$$\mathrm{tr}\left(L_B^\dagger L_G\right) \geq \sum_{i=2}^{N} \frac{\lambda_i^G}{\lambda_i^B}. \tag{20}$$

(See, for example, [31] for a proof.) In the case of identical line ratios, equality holds, and each eigenvalue ratio is equal to α. The unbounded growth of the transient resistive losses with the network size N, which was noted in the special case of (18), is also evident in the bound in (20). In particular, the scaling with network size is evident because the number of eigenvalues and, thus, the sum of their ratios, grows with each added node. We illustrate this growth and the tightness of the bound in (20) through the examples in Section V-B.

The inequality (20) also provides some insight into why the $\mathcal{H}_2$ norm does not have a strong dependence on network connectivity even for networks of nonidentical line ratios. Although the eigenvalues of the Laplacian are difficult to characterize precisely for general graphs, it is well known that they relate strongly to the node degrees (see, for example, [32] and [33]). In (20), however, we consider the ratio between the eigenvalues of L_G and L_B. Since these are two graph Laplacians describing the same topology, their node degrees g_{ii} and b_{ii} can be related through $\bar{\alpha}_i$, the average ratio of line conductances to susceptances of the lines incident to node i. This $\bar{\alpha}_i$ is independent of how many such incident lines there are. It is therefore reasonable to infer that each eigenvalue ratio λ_i^G/λ_i^B is also more strongly related to $\bar{\alpha}_i$ than the number of lines connected to each node, which would be a measure of the network connectivity. We will further explore this notion through the examples in Section V.

As derived in Section III-C, the resistive losses can can also be bounded as (19), which allows for a simple and convenient analysis of the network. Both sides of this inequality increase unboundedly with N, but the bound becomes loose if the system is heterogenous in terms of the line resistance to reactance ratios. This may be the case if a combined transmission and distribution network is considered, or in cases of highly varying impedance loads. In some cases, it is then better to bound the losses in terms of graph-theoretical quantities. This can be done in the following manner:

$$\lambda_2^G \mathrm{tr}\left(L_B^\dagger\right) \leq \mathrm{tr}\left(L_B^\dagger L_G\right) \leq \frac{\mathrm{tr}(L_G)}{\lambda_2^B} \tag{21}$$

where λ_2^G and λ_2^B are the algebraic connectivities of the graphs weighted by line conductances and susceptances, respectively. See [31]for a proof. It holds that $\lambda_2^G \leq (N/(N-1))g_{ii,\min}$ and $\lambda_2^B \leq (N/(N-1))b_{ii,\min}$, where g_{ii}, b_{ii} are the respective self conductances and susceptances of the nodes (i.e., the respective node degrees). Furthermore, the quantity $\mathrm{tr}(L_B^\dagger)$ is proportional to what we can interpret as the *total effective reactance* of the network, in analogy with the concept of total effective resistance, as recently discussed in, for example, [23] and [34].

By Rayleigh's monotonicity law (see [35]), the total effective reactance can decrease unboundedly by adding lines and increasing line susceptances. However, the algebraic connectivity λ_2 is very small for weakly connected networks and can also be found to decrease with network size. Therefore, while the bounds (21) with λ_2 in the denominator, are accurate for small and well-connected networks, they become loose for the large, sparsely connected (i.e. not Kron-reduced) networks that most often characterize a power grid.

In a more general context, Theorem 3.4 applies to many networks with second-order consensus dynamics, and the $\mathcal{H}_2$ norm can be interpreted as a type of energy measure [27]. Such dynamics may describe several types of mechanical or biological systems [10], which may not have similar topological properties to power systems. In these cases, the bound in (21) may provide a more accurate approximation for the $\mathcal{H}_2$ norm.

B. Systems of Nonidentical Generators

The results derived by considering a grid with identical generators suggest that the losses scale with the network size. In order to put these results in context, it is desirable to understand the extent to which these scaling properties apply to systems of nonuniform generators. In this section, we explore these ideas and use the results from previous sections to gain insight. We begin by examining the special case where one nonuniform generator is added to the network.

From Theorem 3.4, we can deduce that

$$\frac{1}{2\beta_{\max}}\mathrm{tr}\left(L_B^\dagger L_G\right) \leq \|H\|_{\mathcal{H}_2}^2 \leq \frac{1}{2\beta_{\min}}\mathrm{tr}\left(L_B^\dagger L_G\right)$$

where $\beta_{\min} = \min_{i\in\{1,\ldots,N\}} \beta_i$ and $\beta_{\max} = \max_{i\in\{1,\ldots,N\}} \beta_i$. The losses are thus lower and upper bounded by the properties of the most strongly and lightly damped generators, respectively. Some interesting questions that arise from this observation are: 1) How does adding a generator to an existing network affect the total resistive losses? and 2) What are the important parameters in determining this incremental cost? The next result addresses one such scenario.

Lemma 4.1: Consider a network of N generators with transient resistive losses given by $\|\tilde{H}_0\|_{\mathcal{H}_2}^2$. If one connects an additional generator with damping β_{N+1} and inertia M_{N+1} to any node $k \in \{1,\ldots,N\}$ in the existing network by a single link with a line ratio of $\alpha_{k,N+1} = r_{k,N+1}/x_{k,N+1}$, then the new network's losses are given by

$$\|\tilde{H}_1\|_{\mathcal{H}_2}^2 = \|\tilde{H}_0\|_{\mathcal{H}_2}^2 + \frac{1}{2\beta_{N+1}}\,\alpha_{k,N+1}.$$

If the dynamics are as per (17), the additive term is instead $(M_{N+1}^2/2\beta_{N+1})\alpha_{k,N+1}$.

Proof: See the Appendix. ■

This result can be interpreted as follows. The additional losses incurred through the connecting a "light" (low inertia) or well-damped generator are smaller than those incurred due to adding a "heavy" (high inertia) or poorly damped generator. In the face of increasingly distributed generation, this result implies that while the synchronization losses do scale with the network size, the impact of low inertia or small-scale distributed generators is relatively low, compared to that of large conventional generators. This concept is further explored in the example of Section V-C.

While further analytical results for systems with nonidentical generators are not presented in this paper, the numerical example in Section V-D provides further insight into the price of synchrony in networks with nonuniform generation. That example shows that although the scaling relationships and topology independence results for the special cases discussed herein hold for limited parameter variations, judicious sizing and placement of new generators can, in fact, reduce system losses.

Remark 4: While results in this paper are only valid for Kron-reduced networks of synchronous generators modeled by second-order swing equations, ongoing work [36] indicates that the main results presented in this paper extend to more general systems. That work employs an extended, structure-preserving network model with load dynamics and asynchronous generators. The similarity in the results of that work imply that the Kron-reduction of the network employed here does not account for the network scaling properties or the weak topological dependence of the transient losses observed herein.

V. Numerical Examples

The results derived and discussed in the previous sections indicate that the price of synchrony in a network of generators with a particular structure is highly dependent on the number of generators in the system. These transient resistive losses were also shown to depend on the system's resistance to reactance ratios and the generator properties as well as to weakly depend on the network topology. In this section, we provide some numerical examples to illustrate these results and to explore more general networks.

A. Line Ratio Variance

We first investigate the behavior of transient resistive losses in systems with increasingly nonuniform network line ratios. In particular, we consider a hypothetical set of identical generators ($\beta = 1$) placed at each node of the IEEE 14-bus, 30-bus, and 57-bus benchmark topologies [37]. We obtain values for the reactances x_{ij} for each $\mathcal{E}_{ij} \in \mathcal{E}$ from the benchmark system data [37]. We then define a series of heterogeneous line ratios by setting $r_{ij} = \alpha_{ij} x_{ij}$, such that $\alpha_{ij} = r_{ij}/x_{ij} = g_{ij}/b_{ij}$ are randomly drawn from uniform distributions on the following range of intervals 0.4, 0.4 $\pm$ 0.025, 0.4 $\pm$ 0.05, ..., 0.4 $\pm$ 0.2. Fig. 2 shows the resistive losses computed from the result in Theorem 3.4 for a number of these systems. The horizontal axis indicates the standard deviation of the line ratios, and the bars represent the upper and lower bounds of the inequality (19).

Fig. 2 shows that increasing the standard deviation of the line ratios leads to a looser bound in (19). However, the resistive losses of the system themselves show only small variations as long as the average line ratio remains constant. Fig. 2 also demonstrates that the transient losses strongly depend on the network size (here 14, 30, or 57 nodes), which is consistent with the relationship in (18). The small changes in the value of the norm as the variance of the parameters is increased can also be understood by considering Theorem 3.4 with the conductance matrix decomposed as $L_G = \alpha L_B + \bar{L}_G$. Then, (16) can be rewritten as

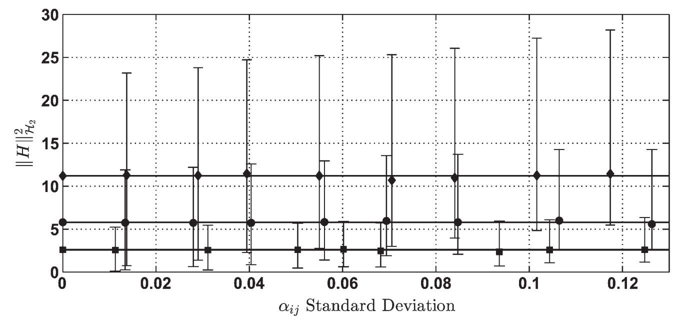

Fig. 2. Transient resistive losses in modified IEEE 14 (bottom), 30 (middle), and 57 (top) bus benchmark networks, randomly generated with lines of increasingly varied random ratios $\alpha_{ij} = r_{ij}/x_{ij}$. The bars illustrate the bounds in (19).

$$\|H\|^2_{\mathcal{H}_2} = \frac{\alpha}{2\beta}(N-1) + \frac{1}{2\beta}\mathrm{tr}\left(L_B^\dagger \bar{L}_G\right)$$

which shows that the deviation from the result based on equal line ratios depends on the size of $\mathrm{tr}(L_B^\dagger \bar{L}_G)$. In Fig. 2, this quantity is illustrated through the small deviations of the computed norm values (round markers) from the horizontal lines representing equal line ratios. For a meaningful choice of α, such as the average line ratio, the entries of $\bar{L}_G$ will take on positive and negative values, small in magnitude but increasing as the variance in line ratios increases. Since $\bar{L}_G$ is in the numerator of the generalized ratio $\mathrm{tr}(L_B^\dagger \bar{L}_G)$, the value of this ratio will be small. A formal proof of this fact as well as the development of a closed-form expression for the expectation values of the transient resistive losses subject to different probability distributions of the line ratios are topics of ongoing research.

B. Network Scaling for Topology Extremes

According to our results, the transient resistive losses incurred in resynchronizing a network of identical generators increase unboundedly with the network size but are only weakly dependent on the network topology. These losses also depend on the ratio between susceptances and reactances of the lines of the Kron-reduced network. In this example, we will compare the $\mathcal{H}_2$ norm in (16) and the bounds discussed in Section IV for systems with underlying graphs that are radial and complete as their respective system sizes increase. These two topologies are chosen because they represent the two extremes with respect to connectivity and, therefore, provide insight into how the transient loss relations described in the previous sections relate to network topology.

We simplify the problem by assuming $\beta = 1$ and then assign random line parameters to each line in the following manner. We draw the line reactance x_{ij} and line ratio α_{ij} from a

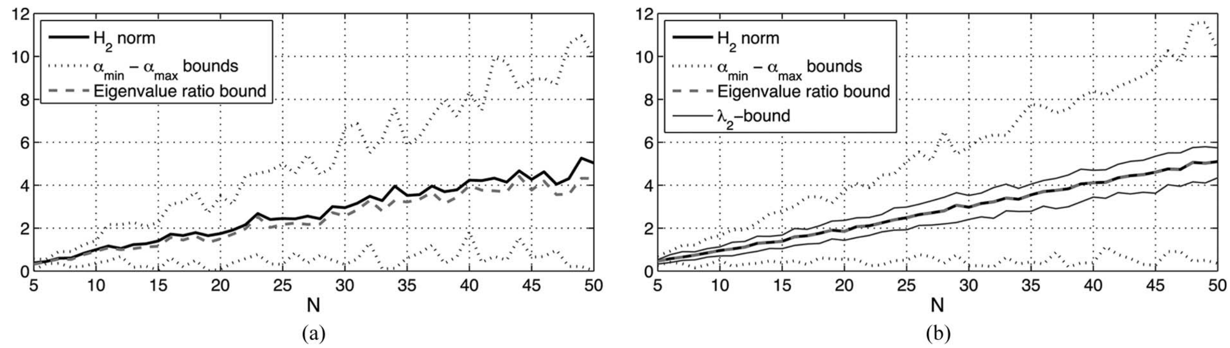

Fig. 3. $\mathcal{H}_2$ norms for (a) a line graph and (b) a complete graph network of N nodes, with some of the bounds discussed in Section IV. Despite some variation due to the randomness in the line parameters, the $\mathcal{H}_2$ norm scales directly with the network size and is roughly the same for the radial as for the complete graph. The bound related to the Laplacian eigenvalue ratios (20) is the most accurate bound, and for the complete graph, the inequality (21) is linked to the algebraic connectivity λ_2, also provides accurate bounds (for the radial graph, the latter have been omitted since they are off by orders of magnitude due to small connectivity).

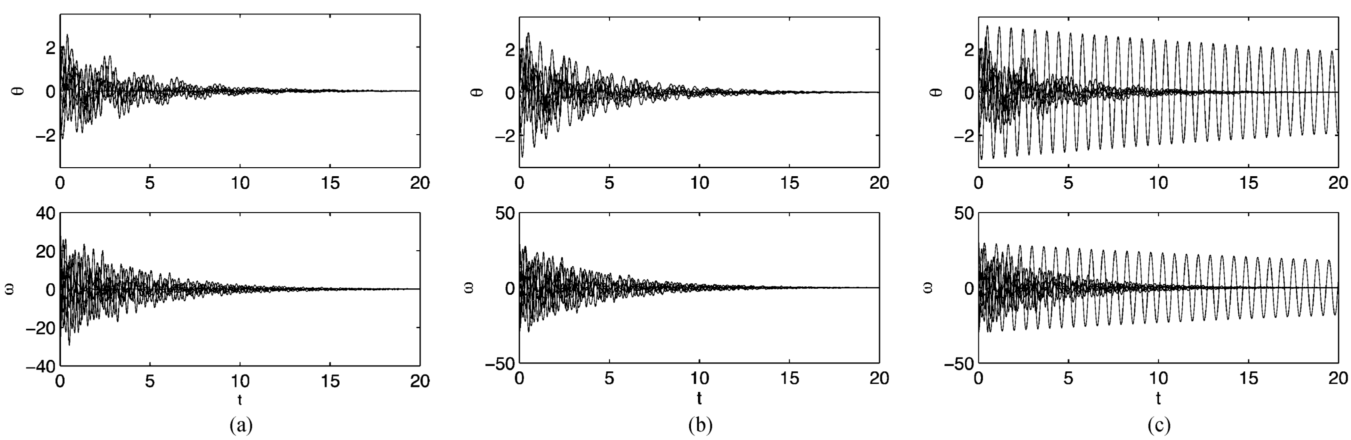

Fig. 4. Simulation of the 7-bus network of Fig. 1 with identical generators, a grounded node, and an additional (eighth) generator with (a) 10 times, (b) the same, and (c) a tenth of the damping of the other generators. This generator is connected to the grounded node number 1. The system is subject to random velocity and zero-phase initial conditions, so that the expected power losses correspond to the $\mathcal{H}_2$ norm. The losses are the largest in system (c), where the lightly damped generator maintains its oscillation for a very long time, as predicted by Lemma 4.1.

normal distribution with mean 0.2 and standard deviation 0.1 (any negative values are replaced with the mean). As shown in the previous example, one can then expect the norm for each network to lie close to the result of (18), based on the mean ratio $\bar{\alpha} = 0.2$ and the number of nodes N.

Fig. 3 shows how the norm increases for the line and complete graph systems as the network sizes increase from 5-node to 50-node systems, with the bounds (19), (20) indicated on both panels. Due to space constraints, we show the bounds in (21) only in Fig. 3(b) since this bound is much tighter in the case of complete graphs. For both types of networks, the eigenvalue ratio in (20) provides the tightest bound and grows with N in the same fashion as the norm in (16). We also note that the network-parameter-dependent bounds in (21) are more accurate than the line ratio bounds in (19) for the complete graph.

C. Generator Parameter Dependence of Incremental Losses

We now characterize a particular case of a system with nonuniform generators by examining the situation described in the conditions of Lemma 4.1. For this example, we simulate the 7-bus network depicted in Fig. 1 and set the impedances of all lines $\mathcal{E}_{ij} \in \mathcal{E}$ in this network to $z_{ij} = z_0 = 0.04 + \mathbf{j}0.2$. We let node 1 be the grounded node, and assign to all generators $i = 2, \ldots, N = 7$ the parameters [38]: $M_i = 20/2\pi f$ and $\beta_i = 10/2\pi f = \beta_0$ with a frequency $f = 60$ Hz for all i. We denote this base system as $\tilde{H}_0$.

We then compare the losses that arise from connecting three different generators to node 1. The three generators have $\beta_{N+1} = \beta_8 = 0.1\beta_0,\ \beta_0$, and $10\beta_0$, respectively, and the connecting line has impedance $z_{1,8} = z_0$. Fig. 4 shows the system trajectories of the three resulting reduced systems $\tilde{H}_1$, when they are subjected to a random initial angular velocity disturbances, corresponding to the $\mathcal{H}_2$ norm interpretation 2) in Section II-B.

The expected power losses during the transient response for these respective systems are given by Lemma 4.1 as $\|\tilde{H}_1\|_{\mathcal{H}_2}^2 = \|\tilde{H}_0\|_{\mathcal{H}_2}^2 + (\alpha_{1,8}/2\beta_8) = 60.3, 26.4$, and 23.0, respectively. For the particular system trajectories shown in Fig. 4, the losses are respectively 110, 32.2, and 23.7. The weakly damped generator will experience strong oscillations and incur large losses before it stabilizes at the same state as the grounded node. The system that has a new highly damped generator incurs less oscillations and lower transient losses than the system where an identical generator is connected in the same location.

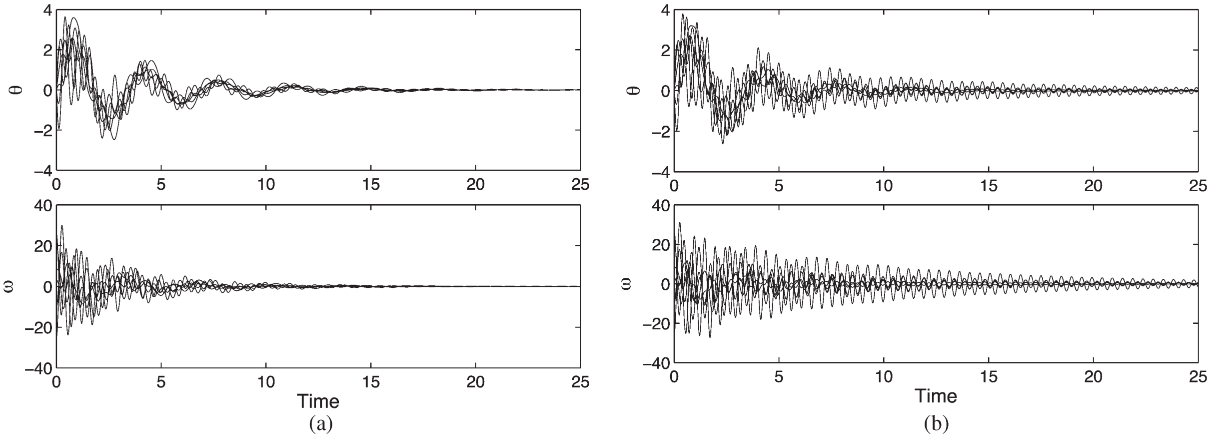

Fig. 5. Simulation of oscillations in the reduced 7-bus system in Fig. 1 with node 1 grounded and (a) the strongly damped generators placed at the most highly interconnected nodes, and (b) the strongly damped generators placed at the most weakly interconnected nodes. The system in (b) is less coherent and experiences larger resistive losses during the transient response: 27.9 compared to 13.2 in system (a) for these particular trajectories.

D. Networks With Nonuniform Generators

Our final example further relaxes the assumption of equal generator parameters. Consider the network depicted in Fig. 1 with equal line impedances $z_{ij} = r_{ij} + \mathbf{j}x_{ij} = 0.1 + \mathbf{j}0.6$. In this network, nodes 1 and 7 have the smallest node degree which we denote D_1. Node 4 then has degree $4D_1$, nodes 2 and 6 have degree $3D_1$, and nodes 3 and 5 both have degree $2D_1$. We set the generator parameters to $M = 20/2\pi f$ for all nodes, but let the damping $\beta \in (1/2\pi f)\{2,\ 8,\ 14,\ 20\}$ vary for each of the four types of nodes, that is, nodes having degrees D_1, $2D_1$, $3D_1$, or $4D_1$.

We study this system under two conditions: (a) the strongly damped generators are placed at highly connected nodes (i.e., matched dampings and degrees) and (b) strongly damped generators are placed at the least connected nodes (i.e., mismatched dampings and degrees). We define $\tilde{H}_{\mathrm{match}}$ as the system corresponding to a network where the node degrees have been matched to the size of the damping coefficients β (i.e., $\beta_i = 2$ at nodes with degree D_1, $\beta_i = 8$ at nodes with degree $2D_1$, $\beta_i = 14$ at nodes with degree $3D_1$, and $\beta_i = 20$ at nodes with degree $4D_1$) as in condition (a). We then denote the system corresponding to a network where the degrees and damping are mismatched as in condition (b) as $\tilde{H}_{\mathrm{mismatch}}$.

These systems are subjected to a random initial angular velocity disturbance in the manner described in Section V-C. This leads to the expected transient power losses $\|\tilde{H}_{\mathrm{match}}\|_{\mathcal{H}_2}^2 = 18.9$ and $\|\tilde{H}_{\mathrm{mismatch}}\|_{\mathcal{H}_2}^2 = 20.7$. These results indicate that there are lower losses for the system corresponding to case (a) where the dampings are matched to the nodal degrees.

Fig. 5 shows the state trajectories of the two systems for a particular input sequence. For this particular example, the transient behavior of the system $\tilde{H}_{\mathrm{mismatch}}$ is clearly less "coherent" than that of $\tilde{H}_{\mathrm{match}}$. In addition, since the connectivity of the graph underlying these networks is identical, the additional oscillations in the phase angle will lead to increased transient losses. This observation is verified when we compute the respective losses for the particular trajectories shown. These are 13.2 for the matched case in Fig. 5(a) and 27.9 for the mismatched case in Fig. 5(b). These results and similar case studies have led us to conclude that for systems with nonuniform generator parameters, judicious network design that places well-damped generators at highly interconnected nodes can reduce transient power losses. An intuitive explanation to this is that a well-damped generator is able to exert a larger effect on the entire network if it is well connected than if it is remotely located. However, note that although we are considering an extreme case where the best damped generator has as much as a 10 times larger damping coefficient than the most poorly damped one, the total expected value for the transient losses only differ by 10% between the most optimal and least optimal generator arrangement for the particular example topology.

VI. Conclusion

We quantified the resistive line losses that occur due to the power flows required to maintain synchrony in a power network in the presence of persistent disturbances or transient events. These losses are the cost of using power flow through transmission lines as the signaling mechanism for synchronization control, which motivates the term "price of synchrony." In the special case of identical generators, we derived a formula for the total transient losses expressed as a generalized ratio of the weighted graph Laplacians representing the conductance and susceptance matrices. We showed that this quantity generally scales unboundedly with the number of nodes (generators) in the system. For the special case where all of the transmission lines have equal conductance to susceptance ratios, we showed that the total transient resistive losses are independent of network topology and directly proportional to the number of nodes in the network. This topological independence implies that while the highly connected network may have better phase coherence and transient stability properties than a loosely connected one, the two types are equivalent in terms of the transient power losses required to maintain that coherence. While this conclusion may at first seem surprising, it becomes fairly intuitive when one considers the following contrast between highly versus sparsely connected networks. A highly connected and, therefore, highly phase-coherent network has much smaller phase fluctuations than a loosely connected one. Therefore, while the "per-link" resistive losses are smaller in the former, it has many more links than the latter and, thus, the total losses summed over all links are the same for both networks. While ongoing work [36] shows that the scaling relationships are retained in network-preserving model with load and asynchronous generator dynamics, an important future research question is to determine the extent to which these results can be extended to general power networks.

The results we present have some interesting implications for the design of future power grids, which are expected to be highly distributed. In particular, they indicate that transient losses can grow unboundedly with network size. In addition, the results indicate that this growth is unlikely to be mitigated by increasing network coherence through additional transmission linkages, unless these linkages focus on an optimal matching of generator damping to the nodal degree. Such strategic addition of generation at highly connected nodes may be impractical for an existing system or when connecting new distributed generation. These results point to a fundamental limitation to a system where power flow (either in an open-loop system or as regulated through a control device) is the mechanism by which the system resynchronizes or maintains this state. The analysis provided in this work may be particularly relevant to future power networks that are likely to have orders of magnitude more generators than today's networks. In fact, these results can be construed as an additional argument in support of investigating the use of communication links (for phase and frequency information) as an additional means of stabilizing control in power networks.

Appendix

Proof of Lemma 3.2

Consider the following state transformation of the system (9):

$$\begin{bmatrix}\theta\\ \omega\end{bmatrix} =: \begin{bmatrix}U & 0\\ 0 & U\end{bmatrix}\begin{bmatrix}\theta'\\ \omega'\end{bmatrix}$$

where U is the unitary matrix which diagonalizes L_B, that is, $U^*L_BU = \Lambda_B = \mathrm{diag}\{0,\ \lambda_2^B, \dots, \lambda_N^B\}$, where $0 = \lambda_1^B \leq \lambda_2^B \leq \ldots \leq \lambda_N^B$ are the eigenvalues of L_B. We have assumed, without loss of generality, that $U = [(1/\sqrt{N})\mathbf{1}\ \ u_2\ \dots\ u_N]$, where u_i, for $i = 2, \dots, N$ are the eigenvectors corresponding to the aforementioned eigenvalues.

Since the $\mathcal{H}_2$ norm is unitarily invariant, we can also define $\mathrm{w}' = U^*\mathrm{w}$ and $y' = U^*y$ to obtain the system

$$\frac{d}{dt}\begin{bmatrix}\theta'\\ \omega'\end{bmatrix} = \begin{bmatrix}0 & I\\ -\frac{1}{M}\Lambda_B & -\frac{\beta}{M}I\end{bmatrix}\begin{bmatrix}\theta'\\ \omega'\end{bmatrix} + \begin{bmatrix}0\\ \frac{1}{M}I\end{bmatrix}\mathrm{w}'$$
$$y' = \begin{bmatrix}U^*L_G^{\frac{1}{2}}U & 0\end{bmatrix}\begin{bmatrix}\theta'\\ \omega'\end{bmatrix}. \tag{22}$$

Now, observe that

$$U^*L_GU = \begin{bmatrix}0 & \cdots & 0\\ \vdots & \hat{L}_G & \\ 0 & & \end{bmatrix} \tag{23}$$

which implies that the first rows and columns of U^*L_GU and Λ_B are zero. We thus have that the states $\theta_1' = (1/\sqrt{N})\sum_{i=1}^N \theta_i$ and $\omega_1' = (1/\sqrt{N})\sum_{i=1}^N \omega_i$ satisfy the dynamics

$$\dot{\theta}_1' = \omega_1' \tag{24a}$$
$$\dot{\omega}_1' = -\frac{\beta}{M}\omega_1' + \frac{1}{M}\mathrm{w}_1' \tag{24b}$$
$$y_1' = 0. \tag{24c}$$

Equation (24) reveals that the associated mode, which corresponds to the single zero eigenvalue of L_B, is unobservable from the output. We denote the system associated with the this mode as H_1'. The remaining eigenvalues of the system (22) lie strictly in the left half of the complex plane because L_B is positive semidefinite. It follows that the input–output transfer function from w' to y' is stable and has finite $\mathcal{H}_2$ norm.

By the equivalence of this system and H, we have thus established the existence of the $\mathcal{H}_2$ norm for the system H.

We can now partition the system into the subsystems H_1' and $\hat{H}$. We take $\hat{L}_G$ as the Hermitian positive definite submatrix in (23) and define $\hat{\Lambda}_B = \mathrm{diag}\{\lambda_2^B,\ \lambda_3^B, \dots, \lambda_N^B\}$ and write the input–output mapping $\hat{H}$ as

$$\frac{d}{dt}\begin{bmatrix}\hat{\theta}\\ \hat{\omega}\end{bmatrix} = \begin{bmatrix}0 & I\\ -\frac{1}{M}\hat{\Lambda}_B & -\frac{\beta}{M}I\end{bmatrix}\begin{bmatrix}\hat{\theta}\\ \hat{\omega}\end{bmatrix} + \begin{bmatrix}0\\ \frac{1}{M}I\end{bmatrix}\hat{\mathrm{w}}$$
$$\hat{y} = \begin{bmatrix}\hat{L}_G^{\frac{1}{2}} & 0\end{bmatrix}\begin{bmatrix}\hat{\theta}\\ \hat{\omega}\end{bmatrix} \tag{25}$$

or $\Leftrightarrow \frac{d}{dt}\tilde{\phi} = A\tilde{\phi} + B\hat{\mathrm{w}};\ \tilde{y} = C\tilde{\phi}$.

Note that the systems $\hat{H}_1$ and $\tilde{H}$ are completely decoupled and we therefore have that $\|H\|_{\mathcal{H}_2}^2 = \|H_1'\|_{\mathcal{H}_2}^2 + \|\hat{H}\|_{\mathcal{H}_2}^2 = \|\hat{H}\|_{\mathcal{H}_2}^2$.

The $\mathcal{H}_2$ norm can then be calculated in perfect analogy to the derivations in Section III-B and we obtain that

$$\|H\|_{\mathcal{H}_2}^2 = \frac{1}{2\beta}\mathrm{tr}\left(\hat{\Lambda}_B^{-1}\hat{L}_G\right). \tag{26}$$

Now, we show that the result of Lemma 3.1 can be written in terms of the state transformed matrices $\hat{\Lambda}_B$ and $\hat{L}_G$. Define the $N \times (N-1)$ and the $(N-1) \times N$ matrices R and P by

$$R = \begin{bmatrix}0 & \cdots & 0\\ & I_{N-1} & \\ & & \end{bmatrix},\ P = \begin{bmatrix}I_{k-1} & & 0\\ & -\mathbf{1} & \\ 0 & & I_{N-k}\end{bmatrix}$$

where k is the index of the grounded node and $-\mathbf{1}$ is the $(N-1) \times 1$ vector with all entries equal to -1. By this design, $\hat{\Lambda}_B = R^*\Lambda_BR$, $\hat{L}_G = R^*U^*L_GUR$, and $L_{B/G} = P^*\tilde{L}_{B/G}P$. Further, to simplify the notation, we define the $(N-1) \times (N-1)$ nonsingular matrix $V = PUR$. Then, we can write

$$\mathrm{tr}\left(\tilde{L}_B^{-1}\tilde{L}_G\right) = \mathrm{tr}\left(VV^{-1}\tilde{L}_B^{-1}(V^*)^{-1}V^*\tilde{L}_G\right)$$

since $VV^{-1} = (V^*)^{-1}V^* = I$. By the cyclic properties of the trace

$$\mathrm{tr}\left(VV^{-1}\tilde{L}_B^{-1}(V^*)^{-1}V^*\tilde{L}_G\right) = \mathrm{tr}\left(V^{-1}\tilde{L}_B^{-1}(V^*)^{-1}V^*\tilde{L}_GV\right)$$
$$= \mathrm{tr}\left(\left(V^*\tilde{L}_BV\right)^{-1}V^*\tilde{L}_GV\right).$$

But $V^*\tilde{L}_BV = R^*U^*P^*\tilde{L}_BPUR = \hat{\Lambda}_B$ and $V^*\tilde{L}_GV = R^*U^*P^*\tilde{L}_GPUR = \hat{L}_G$. Hence

$$\mathrm{tr}\left(\tilde{L}_B^{-1}\tilde{L}_G\right) = \mathrm{tr}\left(\hat{\Lambda}_B^{-1}\hat{L}_G\right).$$

In conclusion

$$\|H\|^2_{\mathcal{H}_2} = \frac{1}{2\beta}\mathrm{tr}\left(\hat{\Lambda}_B^{-1}\hat{L}_G\right) = \frac{1}{2\beta}\mathrm{tr}\left(\tilde{L}_B^{-1}\tilde{L}_G\right) = \|\tilde{H}\|^2_{\mathcal{H}_2}$$

which proves the Lemma.

Proof of Lemma 3.3

By the proof of Lemma 3.2, we have that $\mathrm{tr}(\tilde{L}_B^{-1}\tilde{L}_G) = \mathrm{tr}(\hat{\Lambda}_B^{-1}\hat{L}_G)$. Now

$$\mathrm{tr}\left(\hat{\Lambda}_B^{-1}\hat{L}_G\right) = \mathrm{tr}\left(\begin{bmatrix} 0 & 0 \\ 0 & \hat{\Lambda}_B^{-1}\hat{L}_G \end{bmatrix}\right) = \mathrm{tr}\left(\begin{bmatrix} 0 & 0 \\ 0 & \hat{\Lambda}_B^{-1} \end{bmatrix} U^*L_GU\right).$$

By definition, see, for example, [39], $U^*L_B^{\dagger}U = \mathrm{diag}\{0, 1/\lambda_2^B, \ldots, 1/\lambda_N^B\}$, which makes the above equivalent to $\mathrm{tr}(U^*L_B^{\dagger}UU^*L_GU) = \mathrm{tr}(U^*L_B^{\dagger}L_GU)$. But since the trace is unitarily invariant, it follows that:

$$\mathrm{tr}\left(\hat{\Lambda}_B^{-1}\hat{L}_G\right) = \mathrm{tr}\left(L_B^{\dagger}L_G\right)$$

which concludes the proof.

Proof of Lemma 4.1

Without loss of generality, choose the node the new generator is connected to as the grounded node, and denote it by N. Let $\tilde{\mathcal{M}} := \mathrm{diag}\{M_1, \ldots, M_N\}$, $\tilde{\mathcal{B}} = \mathrm{diag}\{\beta_1, \ldots, \beta_N\}$, and denote the new $(N+1)$th node as NI for notational compactness. The reduced system $\tilde{H}_1$ can then be written as

$$\frac{\mathrm{d}}{\mathrm{d}t}\begin{bmatrix} \tilde{\theta} \\ \theta_{NI} \\ \tilde{\omega} \\ \omega_{NI} \end{bmatrix} = \begin{bmatrix} \mathbf{0} & \mathbf{0} & I_N & \mathbf{0} \\ \mathbf{0} & \mathbf{0} & \mathbf{0} & 1 \\ -\tilde{\mathcal{M}}^{-1}\tilde{L}_B & \mathbf{0} & -\tilde{\mathcal{M}}^{-1}\tilde{\mathcal{B}} & \mathbf{0} \\ \mathbf{0} & -\frac{b_{N,NI}}{M_{NI}} & \mathbf{0} & -\frac{\beta_{NI}}{M_{NI}} \end{bmatrix} + \begin{bmatrix} \mathbf{0} & \mathbf{0} \\ \mathbf{0} & 0 \\ \tilde{\mathcal{M}}^{-1} & \mathbf{0} \\ \mathbf{0} & \frac{1}{M_{NI}} \end{bmatrix}\begin{bmatrix} \tilde{\mathrm{w}} \\ \mathrm{w}_{NI} \end{bmatrix}$$

$$\begin{bmatrix} \tilde{y} \\ y_{NI} \end{bmatrix} = \begin{bmatrix} \tilde{L}_G^{\frac{1}{2}} & \mathbf{0} & \mathbf{0} & \mathbf{0} \\ \mathbf{0} & \sqrt{g_{N,NI}} & \mathbf{0} & 0 \end{bmatrix}\begin{bmatrix} \tilde{\theta} \\ \theta_{NI} \\ \tilde{\omega} \\ \omega_{NI} \end{bmatrix}. \tag{27}$$

Let the input–output mapping H_{NI} be the SISO subsystem of (27)

$$\frac{\mathrm{d}}{\mathrm{d}t}\begin{bmatrix} \theta_{NI} \\ \omega_{NI} \end{bmatrix} = \begin{bmatrix} 0 & 1 \\ -\frac{b_{N,NI}}{M_{NI}} & -\frac{\beta_{NI}}{M_{NI}} \end{bmatrix}\begin{bmatrix} \theta_{NI} \\ \omega_{NI} \end{bmatrix} + \begin{bmatrix} 0 \\ \frac{1}{M_{NI}} \end{bmatrix}\mathrm{w}_{NI}$$

$$y_{NI} = \begin{bmatrix} \sqrt{g_{N,NI}} & 0 \end{bmatrix}\begin{bmatrix} \theta_{NI} \\ \omega_{NI} \end{bmatrix}.$$

From (27), it is clear that the systems $\tilde{H}_0$ and H_{NI} are entirely decoupled and since we can write $\tilde{H}_1 = \mathrm{diag}\{\tilde{H}_0, \tilde{H}_1\}$

$$\|\tilde{H}_1\|^2_{\mathcal{H}_2} = \|H_0\|^2_{\mathcal{H}_2} + \|H_{NI}\|^2_{\mathcal{H}_2}.$$

Now, the $\mathcal{H}_2$ norm of H_{NI} can be calculated in scalar analogy to the derivation in Section III-B to yield

$$\|H_{NI}\|^2_{\mathcal{H}_2} = \frac{1}{2\beta_{NI}}\frac{g_{N,NI}}{b_{N,NI}} = \frac{\alpha_{N,NI}}{2\beta_{NI}}$$

which concludes the proof.

Acknowledgment

The authors would like to thank H. Sandberg of KTH Royal Institute of Technology for his insightful comments and a number of interesting discussions.

References

[1] "Annual energy outlooks 2010 with projections to 2035," U.S. Dept. of Energy, Tech. Rep. DOE/EIA-0383, 2010. [Online]. Available: http://www.eia.doe.gov/oiaf/aeo

[2] B. Roberts and C. Sandberg, "The role of energy storage in development of smart grids," *Proc. IEEE*, vol. 99, no. 6, pp. 1139–1144, Jun. 2011.

[3] "Power systems of the future: The case for energy storage, distributed generation, and microgrids," IEEE Smart Grid, Tech. Rep., Nov. 2012. [Online]. Available: http://smartgrid.ieee.org/images/features/smart_grid_survey.pdf

[4] P. Kundur *et al.*, "Definition and classification of power system stability IEEE/CIGRE joint task force on stability terms and definitions," *IEEE Trans. Power Syst.*, vol. 19, no. 3, pp. 1387–1401, Aug. 2004.

[5] A. E. Motter, S. A. Myers, M. Anghel, and T. Nishikawa, "Spontaneous synchrony in power-grid networks," *Nat. Phys.*, vol. 9, no. 3, pp. 191–197, Feb. 2013.

[6] M. A. Pai, *Power System Stability by Lyapunov's Method*. Amsterdam, The Netherlands: North Holland, 1981.

[7] P. Varaiya, F. Wu, and R.-L. Chen, "Direct methods for transient stability analysis of power systems: Recent results," *Proc. IEEE*, vol. 73, no. 12, pp. 1703–1715, Dec. 1985.

[8] H.-D. Chiang, F. Wu, and P. Varaiya, "Foundations of the potential energy boundary surface method for power system transient stability analysis," *IEEE Trans. Circuits Syst. I, Reg. Papers*, vol. 35, no. 6, pp. 712–728, Jun. 1988.

[9] F. Dörfler and F. Bullo, "Kron reduction of graphs with applications to electrical networks," *IEEE Trans. Circuits Syst. I, Reg. Papers*, vol. 60, no. 1, pp. 150–163, Jan. 2013.

[10] F. Dörfler, M. Chertkov, and F. Bullo, "Synchronization in complex oscillator networks and smart grids," *Proc. Nat. Acad. Sci.*, vol. 110, no. 6, pp. 2005–2010, 2013.

[11] H.-D. Chiang, *Direct Methods for Stability Analysis of Electric Power Systems: Theoretical Foundation, BCU Methodologies, Applications*. Hoboken, NJ, USA: Wiley, 2011.

[12] F. Dörfler and F. Bullo, "Synchronization and transient stability in power networks and non-uniform Kuramoto oscillators," in *Proc. Amer. Control Conf.*, Baltimore, MD, USA, 2010, pp. 930–937.

[13] F. Dörfler and F. Bullo, "Topological equivalence of a structure-preserving power network model and a non-uniform Kuramoto model of coupled oscillators," in *Proc. 50th IEEE Conf. Dec. Control*, Orlando, FL, USA, 2011, pp. 7099–7104.

[14] F. Dörfler and F. Bullo, "Synchronization and transient stability in power networks and non-uniform Kuramoto oscillators," *SIAM J. Control Optimiz.*, vol. 50, no. 3, pp. 1616–1642, 2012.

[15] F. Dörfler and F. Bullo, "Spectral analysis of synchronization in a lossless structure-preserving power network model," in *Proc. 1st IEEE Int. Conf. Smart Grid Commun.*, Gaithersburg, MD, USA, 2010, pp. 179–184.

[16] A. Bergen and D. Hill, "A structure preserving model for power system stability analysis," *IEEE Trans. Power App. Syst.*, vol. PAS-100, no. 1, pp. 25–35, Jan. 1981.

[17] E. Mallada and A. Tang, "Improving damping of power networks: Power scheduling and impedance adaptation," in *Proc. 50th IEEE Conf. Dec. Control*, Orlando, FL, USA, 2011, pp. 7729–7734.

[18] M. Fardad, F. Lin, and M. R. Jovanović, “Design of optimal sparse interconnection graphs for synchronization of oscillator networks,” *IEEE Trans. Autom. Control*, vol. 59, no. 9, pp. 2457–2462, Sep. 2014.

[19] F. Dörfler, M. R. Jovanović, M. Chertkov, and F. Bullo, “Sparsity-promoting optimal wide-area control of power networks,” *IEEE Trans. Power Syst.*, vol. 29, no. 5, pp. 2281–2291, Sep. 2014.

[20] A. von Meier, *Electric Power Systems: A Conceptual Introduction*, E. Desurvire, Ed. Hoboken, NJ, USA: Wiley, 2006.

[21] A. G. Phadke, “Synchronized phasor measurements-a historical overview,” in *Proc. IEEE/Power Energy Soc. Transm. Distrib. Conf. Exhibit.: Asia Pacific*, 2002, vol. 1, pp. 476–479.

[22] U. Miekkala, “Graph properties for splitting with grounded Laplacian matrices,” *BIT*, vol. 33, no. 3, pp. 485–495, 1993.

[23] A. Ghosh, S. Boyd, and A. Saberi, “Minimizing effective resistance of a graph,” *SIAM Rev.*, vol. 50, no. 1, pp. 37–66, Feb. 1988.

[24] M. A. Pai, *Energy Function Analysis for Power System Stability*. Norwell, MA, USA: Kluwer, 1989.

[25] K. Purchala *et al.*, “Usefulness of DC power flow for active power flow analysis,” in *Proc. IEEE PES Gen. Meeting*, 2005, pp. 2457–2462.

[26] B. Bamieh, M. R. Jovanovic, P. Mitra, and S. Patterson, “Coherence in large-scale networks: Dimension-dependent limitations of local feedback,” *IEEE Trans. Autom. Control*, vol. 57, no. 9, pp. 2235–2249, Sep. 2012.

[27] M. Siami and N. Motee, “Fundamental limits on robustness measures in networks of interconnected systems,” in *Proc. IEEE 52nd Annu. Conf. Dec. Control*, Dec. 2013, pp. 67–72.

[28] L. Freris and D. Infield, *Renewable Energy in Power Systems*. Chichester, U.K.: Wiley, 2008.

[29] B. Bamieh and D. Gayme, “The price of synchrony: Resistive losses due to phase synchronization in power networks,” in *Proc. Amer. Control Conf.*, Jun. 2013, pp. 5815–5820.

[30] L. Pecora and T. Carroll, “Master stability functions for synchronized coupled systems,” *Phys. Rev. Lett.*, vol. 80, no. 10, pp. 2109–2112, 1998.

[31] F. Zhang and Q. Zhang, “Eigenvalue inequalities for matrix product,” *IEEE Trans. Autom. Control*, vol. 51, no. 9, pp. 1506–1509, Sep. 2006.

[32] F. R. K. Chung, *Spectral Graph Theory*. Providence, RI, USA: Amer. Math. Soc., 1994.

[33] C. Zhan, G. Chen, and L. F. Yeung, “On the distributions of Laplacian eigenvalues versus node degrees in complex networks,” *Phys. A: Stat. Mechan. Appl.*, vol. 389, no. 8, pp. 1779–1788, 2010. [Online]. Available: http://www.sciencedirect.com/science/article/pii/S0378437109010012

[34] W. Ellens, F. Spieksma, P. Van Mieghem, A. Jamakovic, and R. Kooij, “Effective graph resistance,” *Linear Algebra Appl.*, vol. 435, no. 10, pp. 2491–2506, 2011.

[35] P. G. Doyle and J. L. Snell, *Random Walks and Electric Networks.* Washington, DC, USA: The Mathematical Association of America, 1984.

[36] E. Sjödin and D. Gayme, “Transient losses in synchronizing renewable energy integrated power networks,” in *Proc. Amer. Control Conf.*, Jun. 2014, pp. 5217–5223.

[37] “Power Systems Test Case Archive,” University of Washington, Seattle, WA, USA, 1993.

[38] P. Sauer and M. A. Pai, Eds., *Power System Dynamics and Stability*. Upper Saddle River, NJ, USA: Prentice-Hall, 1999.

[39] “Generalized Inverse of the Laplacian matrix and some applications,” *Bull. Classe Sci. Math. Naturelles. Sci. Math.*, vol. 129, no. 29, pp. 15–23, 2004. [Online]. Available: http://eudml.org/doc/125464

Emma Tegling received the M.Sc. degree in engineering physics from KTH Royal Institute of Technology, Stockholm, Sweden, in 2013, where she is currently pursuing the Ph.D. degree in electrical engineering.

In 2013, she was a Visiting Graduate Student in the Department of Mechanical Engineering, Johns Hopkins University, Baltimore, MD, USA. Her current research interests include control of networked systems with a focus on renewable energy integrated power systems.

Bassam Bamieh (M’90–SM’02–F’08) received the B.S. degree in electrical engineering and physics from Valparaiso University, Valparaiso, IN, USA, in 1983, and the M.Sc. and Ph.D. degrees in electrical and computer engineering from Rice University, Houston, TX, USA, in 1986 and 1992, respectively.

From 1991 to 1998, he was an Assistant Professor in the Department of Electrical and Computer Engineering and the Coordinated Science Laboratory of the University of Illinois at Urbana-Champaign. Currently, he is a Professor of Mechanical Engineering at the University of California at Santa Barbara, Santa Barbara, CA, USA. His current research interests are optimal and robust control, distributed/networked systems control, transition and turbulence modeling and control, and thermoacoustic energy conversion devices.

Dr. Bamieh is a recipient of the AACC Hugo Schuck Best Paper Award, the IEEE CSS Axelby Outstanding Paper Award (twice), and a National Science Foundation CAREER Award. He is a Control Systems Society Distinguished Lecturer and a Fellow of IFAC.

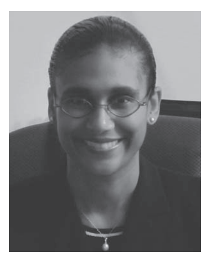

Dennice F. Gayme (M’10–SM’14) received the B.Eng. degree in mechanical engineering from McMaster University, Hamilton, ON, Canada, in 1997, the M.S. degree in mechanical engineering from the University of California at Berkeley, Berkeley, CA, USA, in 1998, and the Ph.D. degree in control and dynamical systems from the California Institute of Technology, Pasadena, CA, USA, in 2010.

Previously, she was a Senior Research Scientist in the Systems and Control Technology and Vehicle Health Monitoring Groups at Honeywell Laboratories in Minneapolis, MN from 1999 to 2003. In 2012, she joined the Mechanical Engineering Department at Johns Hopkins University, Baltimore, MD, USA, where she is currently an Assistant Professor. Her research interests are in the study of large-scale networked and spatially distributed systems in applications, such as power networks, wind farms, and wall turbulence.

Prof. Gayme was a recipient of the P.E.O. scholar award in 2007 and the James Irvine Foundation Graduate Fellowship in 2003.